Published in final edited form as:
Biomaterials. 2014 February ; 35(5): 1367–1377. doi:10.1016/j.biomaterials.2013.10.052.

Three Dimension Filamentous Human Cardiac Tissue Model

Zhen Ma[a,§], **Sangmo Koo**[b,§], **Micaela A. Finnegan**[a], **Peter Loskill**[a], **Nathaniel Huebsch**[c,d], **Natalie C. Marks**[a], **Bruce R. Conklin**[c,d], **Costas P. Grigoropoulos**[b], and **Kevin E. Healy**[a,e,*]

[a] Department of Bioengineering, University of California, Berkeley, CA 94720, USA

[b] Department of Mechanical Engineering, University of California, Berkeley, CA 94720, USA

[c] Gladstone Institute of Cardiovascular Disease, San Francisco, CA 94143, USA

[d] Departments of Medicine and Cellular and Molecular Pharmacology, University of California, San Francisco, CA 94143, USA

[e] Department of Material Science and Engineering, University of California, Berkeley, CA 94720, USA

Abstract

A human *in vitro* cardiac tissue model would be a significant advancement for understanding, studying, and developing new strategies for treating cardiac arrhythmias and related cardiovascular diseases. We developed an *in vitro* model of three-dimensional (3D) human cardiac tissue by populating synthetic filamentous matrices with cardiomyocytes derived from healthy wild-type volunteer (WT) and patient-specific long QT syndrome type 3 (LQT3) induced pluripotent stem cells (iPS-CMs) to mimic the condensed and aligned human ventricular myocardium. Using such a highly controllable cardiac model, we studied the contractility malfunctions associated with the electrophysiological consequences of LQT3 and their response to a panel of drugs. By varying the stiffness of filamentous matrices, LQT3 iPS-CMs exhibited different level of contractility abnormality and susceptibility to drug-induced cardiotoxicity.

Keywords

Induced pluripotent stem cells; cardiac disease model; two-photon initiated polymerization; long QT syndrome; cardiac contractility; drug testing

1. Introduction

Effective treatments for numerous cardiovascular diseases are significant unmet needs, and one significant challenge is the lack of an established *in vitro* model of human cardiac tissue that would be useful for developing and testing potential therapies. Human induced pluripotent stem (iPS) cell technology allows the recapitulation of human disease models *in vitro*, which can be used to both study disease mechanisms and ultimately design and screen

* Corresponding author: Kevin E. Healy Hearst Memorial Mining Building, Room 370 Department of Materials Science and Engineering University of California at Berkeley, Berkeley, CA 94720, United States. Tel.: +1 510 643 3559; Fax: +1 510 643 5792; kehealy@berkeley.edu.
§These two authors equally contribute to this manuscript.

personalized therapeutics prior to large animal or clinical trials. Patient-specific iPS cell-derived cardiomyocytes (iPS-CMs) have been shown to provide valuable models of congenital cardiomyopathies caused by mutations in genes coding for ion channels or ion channel–associated proteins, such as long QT syndrome (LQTS) [1,2]. LQT3, with a mutation in the SCN5a gene, enhances late Na^+ channel currents (I_{Na+}) that fail to inactivate completely and conduct increased inward currents. This prolonged depolarization results in delayed repolarization, a prolonged QT interval, and increases the risk of fatal arrhythmia.

Although genetics play a critical role in the onset of cardiac disease, non-genetic stress – for example, due to forces and paracrine factors normally experienced in the heart, or changes in those cues in the setting of drugs or disease – also makes an important contribution to cardiac pathology. Therefore, developing a "patient/disease-specific" three-dimensional (3D) cardiac model of LQT3 and other cardiac diseases would be a significant advancement for understanding the disease mechanism *in vitro*. Native myocardial tissues are organized into parallel cardiac muscle fibers with aligned intracellular contractile myofibrils and gap junction complexes between contacting CMs, which are important to form the integrated electrical and mechanical properties of human heart. Previous studies on the disease mechanisms of LQT3 and drug screening for treatment were highly dependent on two-dimensional (2D) cell culture, which does not represent the cellular environment within the myocardium [3]. The interplay between gene expression and environmental intricacies causes large functional variations of cells [4-7]. For example, an "*in vivo-like*" microenvironment with aligned CMs has been shown to facilitate mesenchymal stem cells acquisition of cardiac-specific contractile cytoskeleton proteins, transcription factors, gap junction protein distribution, and electrophysiological properties [8]. The substrate stiffness contributed to the maturation of neonatal CMs [9] and regulated sarcomere structure and calcium transient of adult CMs [10].

Previous strategies for generating aligned 3D cardiac tissue relied on the implementation of mechanical loading by pairs of cantilever posts to stretch 3D matrices (collagen I and fibrinogen) mixed with CMs [11,12]. By loading fibrin-based hydrogels mixed with CMs onto microfabricated polydimethylsiloxane (PDMS) molds, others have created a 3D cardiac tissue with aligned structure [13]; however, these animal-derived extracellular matrix (ECM) scaffolds suffer from vial-to-vial variability, inhomogeneous structure, inconsistent reproducibility and lack of precise control over essential scaffold parameters. Others have also successfully electrospun 3D scaffolds with aligned nanofibers using synthetic polymers to structurally mimic the orientation of ECM in the myocardium, which helped CMs self-organize into an anisotropic structure [14]. However, the electrospinning method results in nanoscale and uncontrollable porosity and cannot allow immediate cell infiltration into the matrix to create a true 3D cellular structure. In order to systematically study human stem cell behavior in a 3D environment, more advanced fabrication methods are needed to produce scaffolds with accurately defined micro- and nanoscale features. Two-photon initiated polymerization (TPIP), a laser writing technique based on the phenomenon of two-photon absorption (TPA), can be confined to cure photoresists only near the laser focal volume, enabling fabrication of arbitrary 3D structures with spatial resolution approaching 100 nm [15-17].

With the TPIP technique, we created a bioinspired cardiac tissue model with a cohort of 3D filamentous matrices that precisely regulated the structural alignment of CMs and adjusted the cellular mechanical environment. The filamentous matrices consisted of synthetic parallel fibers with tunable fiber diameter and spacing. The CMs differentiated from LQT3 iPS cells were verified to faithfully recapitulate the electrophysiological abnormality of delayed repolarization. By seeding LQT3 iPS-CMs on such a highly controllable filamentous matrix, we generated a disease-specific 3D cardiac tissue and studied the

contractility malfunctions associated with the electrophysiological consequences of LQT3 syndrome. By the comparison with 2D cell culture, we highlighted the different response of our 3D tissue model to a panel of drugs associated with cardiotoxicity.

2. Materials and methods

2.1 Fabrication of filamentous matrices

The filamentous matrices were fabricated via the TPIP system (Figure 1A) based on a femtosecond laser beam irradiated vertically to the photoresist, a UV-curable organic-inorganic hybrid polymer (ORMOCER®, Micro resist technology). The photoresist were spin-coated onto glass plates (25 mm in length, 3 mm in width, and 1 mm in thickness) at 4000 RPM for 100 seconds, pre-baked on a hotplate at 80°C for 2 minutes, and cured by UV light illumination for 30 minutes. Two glass plates were assembled with two 0.5 mm-thick spacers at the ends and subsequently hard baked at 140°C fo r 1.5 hour. The assembled glass scaffold was filled by uncured photoresist and placed on PC-controllable X-Y-Z motorized stages (Aerotech, ANT95-XY-MP and ANT95-50-L-Z-RH) with high precise positioning. Single fibers were fabricated along the laser beam path with a high-repetition rate femtosecond laser irradiation (Movie S1). The femtosecond laser (pulse duration: ~400 fs, repetition frequency: 1 MHz, wavelength: 1045 nm, FCPA μJewel D-400, IMRA America, Inc.) was frequency-doubled to the wavelength of ~522 nm by Lithium triborate (LBO) second harmonic nonlinear crystal (Newlight photonics) and focused onto the glass plate/photoresist interface with a 5X microscope objective (M Plan Apo, N.A. = 0.14, Mitutoyo). The fibers with different diameters could be fabricated by changing the laser power and exposure time. The power of the laser beam emitted downstream of the objective lens was measured by a power meter and controlled by a half-wave plate and a polarizing beam splitter. The exposure time was set by a PC-controllable mechanical shutter. Fibers with diameters of 5 μm and 10 μm were created with powers of 2.6 mW for 0.7 s exposure and 6.4 mW for 1 s exposure respectively. Different fiber spacing within the matrices was controlled by the X-Y-Z stage with high positioning precision operated by a PC. After finishing the polymerization process, the samples were placed on a hotplate at 120°C for 30 min for post-baking. After cooling in the air for 10 min, the matrices were immersed in the developer (ORMODEV®, Micro resist technology) for 1 hour to remove uncured photoresist. To reduce the tendency of adherent between of fibers, the matrices were immersed into the 60 mg/mL asolectin (Sigma Aldrich) solution for 30 min, and then rinsed five times with 2-propanol (Sigma Aldrich) and deionized water by succession. To sterilize the sample, suspended filamentous matrices were immersed in 70% ethanol before usage.

2.2 Cardiac differentiation from iPS cells

The diseased iPS cell line (LQT3) and a healthy cell line counterpart (WT) were obtained from Dr. Conklin's laboratory at the Gladstone Institute of Cardiovascular Research. A small molecule WNT-mediated protocol was used to derive iPS-CMs from these cell lines [18]. Briefly, iPS cells were maintained on 6-well plates coated with Matrigel (BD Biosciences) in mTeSR1 medium (STEMCELL Technologies). On Day -3, cells were dissociated with Accutase (Invitrogen) for 5 min at 37 °C and seeded onto Mat rigel-coated cell culture plates at 25,000 cells/cm^2 in mTeSR1 containing 10 μM Y-27632 (Stemgent). 24 hours later, the medium was changed to mTeSR1 without Y-27632, and cells were maintained in mTeSR1 for two additional days. On Day 0, cells were treated with 12 μM of a GSK3 inhibitor (CHIR9902; Selleckchem) in RPMI 1640 medium containing B27 supplement without insulin (RPMI/B27-I; Life Technologies) for 24 hours. The medium was changed on Day 1 to RPMI/B27-I and incubated for 48 hours, followed by a 48-hour treatment with 5 μM of an inhibitor of Wnt production (IWP-4, Stemgent) beginning on Day

3. On Day 5, the medium was changed to RPMI/B27-I for two days, and then changed to RPMI 1640 containing B27 complete supplement (RPMI/B27-C) on Day 7.

2.3 Generation of 3D cardiac tissue

Each filamentous matrix was placed into one well of a 6-well plate. The matrices were rinsed with Dulbecco's phosphate buffered saline (DPBS, Gibco Invitrogen) three times and coated with 50 μg/mL fibronectin (Sigma Aldrich) in DPBS for 1 hour. The matrices were rinsed with DPBS three times before loading the cells. Sheets of beating CMs were dissociated using a singularization protocol, which included incubation with 1 mg/mL collagenase II (Worthington) with 40 Unit/mL DNase I (BioLabs Inc.) in Hank's balanced salt solution (HBSS) for 1 hour and followed by 0.25% trypsin/EDTA treatment for 5 min at 37°C [19]. The cells were collected, pelleted and resuspended in EB20 media (Knockout DMEM supplemented with 20% fetal bovine serum (FBS), 2mM L-glutamine, 1X MEM non-essential amino acids (MEM-NEAA), 400 nM 2-Mercaptoethanol and 10 μM Y-27632). 500 μL cell suspension with a density of 1 million cells/mL was pipetted over each matrix. After 2 hours, another 4 mL EB20 media was added into each well to cover the whole matrix. The media was switched to RPMI/B27-C the next day to reduce the non-CMs overgrowth and changed every 2 days.

2.4 Immunostaining and microscopy

Cells were characterized using immunostaining and fluorescent microscopy. Samples were fixed with 4% (vol/vol) paraformaldehyde (PFA) for 15 min, permeabilized with 0.2% Triton-X-100 for 5 min, and blocked with 2% BSA, 4% goat serum and 0.1% Triton-X-100 for 30 min. The samples were then incubated with primary antibodies for 2 hours and secondary antibodies for 1.5 hour. DAPI was used to stain cell nuclei in monolayer cell culture and To-Pro-3 was used for filamentous matrices, because the fiber material was auto-fluorescent under UV excitation. For bright-field and epi-fluorescent microscopy, the images were taken using a Nikon Eclipse TS100F microscope with SPOT Flex camera. For confocal microscopy, the images were taken with a Zeiss LSM710 laser-scanning microscope the in Biological Imaging Facility at UC Berkeley. The antibodies used in this study are listed in Table S1.

2.5 Flow cytometry analysis

The pluripotency of iPS cells and efficiency of cardiac differentiation was evaluated using flow cytometry. The iPS cells were dissociated with Accutase and stained using a human pluripotent stem cell multicolor flow cytometry kit against Oct4, SSEA4, and Sox2 (R&D system). Human iPS-CMs were dissociated using the singularization protocol described above, fixed with PFA for 15 min, and incubated with primary antibody (mouse monoclonal cardiac Troponin T, Thermo Scientific) and secondary antibody (Alexa488, Life Technologies) for 30 min each. The labeled cells were analyzed by Guava easyCyte™ Flow Cytometer (EMD Millipore) in the Stem Cell Shared Facility at UC Berkeley.

2.6 RT-qPCR analysis

The expression level of cardiac specific genes was analyzed using RT-qPCR at Day 12. Adherent cells were washed with DPBS and homogenized with 1 mL TRIzol LS reagent (Invitrogen). Total RNA was collected and purified using RNeasy Mini Kit (Qiagen). The total RNA concentration was quantified using a Nanodrop and integrity was determined using the Agilent BioAnalyzer. Conversion of total RNA to cDNA was carried out using SuperScript III Reverse Transcriptase (Invitrogen) with random primers. qPCR was performed on the Applied Biosystems StepOnePlus instrument with customized target arrays in 96-well format (SA Biosciences/Qiagen), using 10 ng cDNA per reaction and

SYBR Green ROX MasterMix (Qiagen). The data was analyzed using $2^{-\Delta Ct}$ method relative to level of the housekeeping gene. The genes used in this study are listed in Table S2.

2.7 Assessment of tissue formation

The formation of 3D cardiac tissue was assessed using fluorescent images from confocal microscopy. The cells penetrating the top layer and spreading on the middle layer were counted by nuclei as N_{CM}, and the total number of fibers within the image was counted as N_F. Thus, the tissue formation was quantified as cells per fiber (N_{CM}/N_F).

2.8 Assessment of iPS-CM alignment

The CM alignment along the fiber direction was assessed with respect to the cell's elongation and orientation in fluorescent images from confocal microscopy. The cell nuclei were measured with transverse diameter (D_t) and conjugate diameter (D_c). The nuclei index representing the cell's elongation was calculated using the ratio of D_c/D_t. The cell's orientation was measured with the acute angle between the fiber direction and nuclei transverse diameter as $\theta (0° \leq \theta \leq 90°)$. The alignment index relative to fiber long axis was calculated by $cos\theta$.

2.9 Assessment of iPS-CM electrophysiology

The CM electrophysiology was assessed with an MEA system (MED64, Alpha MED Scientific Inc). The iPS-CMs on Day 15 were dissociated using the singularization protocol described above and replated on an MEA chip with a density of 1 million cells/mL. The cells were cultured using RPMI/B27-C for 7 days before starting the measurement. During the recording, the cells were maintained at 37°C in a sterile environment. The el ectrical waveform representing the field potential of CMs can export the electrophysiological parameters, including beating frequency (BF), field potential duration (FPD) and field potential amplitude (FPA).

2.10 Assessment of iPS-CM contractility

The CM contractility was assessed based on the recorded video and motion tracking software. The video was taken at 30 f/s and exported as image stacks for motion tracking analysis. The in-house developed motion tracking software, based on block matching algorithms [20], was optimized for tracking CM beating events. This software can identify the contraction and relaxation events during the entire CM beating sequence and export the contractility parameters, including BF, maximal contraction velocity (MCV), maximal relaxation velocity (MRV), and beating duration (BD).

2.11 Fiber stiffness measurement

The fiber stiffness is represented as the elastic modulus (E_f) of the fiber, which can be measured by atomic force microscopy (AFM, XE-100, Park Systems) with tip-less AFM cantilevers (TL-CONT-SPL and TL-FM-SPK, Nanosensors). The shape of fiber is assumed to be a cylinder with circular cross-section, and accordingly the elastic modulus of the fiber with can be calculated by:

$$E_f = \frac{64 K_c d_c l^3}{3\pi D^4 (d_f - d_c)} \quad (1)$$

where l is the fiber length, D is the fiber diameter, d_c is the displacement of the tip-less AFM cantilever, and d_f is the relative deflection of the fiber. The spring constants (K_c) of tip-less AFM cantilevers were determined using the thermal tune method [21] and calculated using AFM software (XEI, Park system).

2.12 Statistical analysis

Data were presented as mean ± SEM. For single comparisons, one-tailed Student's t-test was used. For multiple comparisons, one-way ANOVA was used with Bonferroni post hoc test. $p<0.05$ was considered significant.

3. Results

3.1 Characterization of matrix fabrication

Independent control of matrix parameters is essential for creating an enabling method capable of robust parametric analyses of the effect of each feature on CMs alignment and contractility. The design of filamentous matrices was divided into two classes: (1) constant fiber spacing with varying fiber diameter (5 μm and 10 μm); and, (2) constant fiber diameter with varying fiber spacing (25 μm, 50 μm and 75 μm). Three layers of fibers were fabricated for each matrix to form a 3D structure (Figure 1B). The filamentous matrices with different parameters were defined as "F/Diameter-Spacing". Figure 1C shows a SEM image of an F/10-50 matrix. The fiber stiffness was measured using AFM and listed in Table 1: The fibers within the F/10-50 matrix were about 4 times stiffer than the fiber within the F/5-50 matrix.

3.2 Characterization of cardiac differentiation

The LQT3 and WT iPS cells were seeded as single cells and grown as a monolayer in defined mTeSR1 medium on Matrigel-coated plates. Robust expression of Oct4, Sox2, and SSEA4 were confirmed by flow cytometry on both cell lines (Figure 2A). The LQT3 iPS cells were further characterized by immunostaining with antibodies against Oct4, Nanog, and Sox2 one day after passage (Figure S1A-C), which shown homogeneous expression of these pluripotent markers. The LQT3 cell line was also characterized by cytogenetic analysis and shown to be normal human karyotype of GTG-banding (Figure S1D).

Following the WNT-mediated differentiation protocol, the beating CMs were observed as early as Day 8 and developing CMs formed contracting sheets of cells by day 10 (Movie S2). At Day 12, RT-qPCR analysis showed the upregulation of cardiac specific genes NKX2.5, TNNT2, TNNI3, MYH6, and MYH7 on both LQT3 and WT iPS-CMs (Figure S1E). These sheet-beating CMs stained positive for sarcomeric α-actinin, cardiac troponin T (cTnT), and β-myosin heavy chain (β-MHC, Figure 2B&C). Flow cytometry with antibodies against cTnT demonstrated that the differentiation efficiency of LQT3 and WT cell lines were about 90% CMs and 75% CMs, respectively, in the whole cell population (Figure 2D&E). Using MEA analysis, LQT3 iPS-CMs exhibited prolongation of FPD compared to WT iPS-CMs (Figure 2F&G), equivalent to the longer QT interval in electrocardiography (ECG) measurement. These data verify that LQT3 iPS-CMs can faithfully recapitulate the LQT3 electrophysiological abnormality *in vitro*.

3.3 3D tissue formation and CM alignment

The differentiated sheet-beating CMs were dissociated and seeded directly onto the filamentous matrices. It took three days for iPS-CMs to form the 3D cardiac tissue and restart beating on the fibers. The condensed and aligned cardiac tissue on the filamentous matrix was visualized with cytoskeletal staining for SM22 (Figure 3A). The CMs within the matrices were stained using an antibody against sarcomeric α-actinin specifically, imaged through confocal microscopy and reconstructed as 3D image stacks (Movie S3). Connexin 43 was found between CMs growing on the fibers, ensuring electrical propagation (Figure 3B). 3D tissue formation was quantified by cell per fiber, and CM alignment was measured as nuclei index and alignment index (Figure 3C).

Confocal images of the middle layer of matrices (Figure 3D) were used to assess the 3D tissue formation and CM alignment according to different fiber diameters and spacing. The tissue formation within matrices with 50 μm fiber spacing was significantly larger than the other two types of matrices with 25 μm and 75 μm spacing (Figure 3E). The small fiber spacing, 25 μm, made it difficult for cells to penetrate the top layer and grow on the other layers; therefore, cells on these matrices spread as 2D structure on the top fiber layer, instead of forming a true 3D structure. With the large fiber spacing, 75 μm, the spacing was too large for cells to spread and bridge between adjacent fibers, thus the few cells grew inside the matrices and also failed to form condensed and connected tissue structure. The cells on F/5-50 and F/10-50 matrices were able to form highly connected tissue relative to the fiber backbone.

The matrices with 75 μm spacing had the largest nuclei index and alignment index. The nuclei index of CMs on the 50 μm spacing matrices was significantly larger than 25 μm spacing matrices, but this was not true for alignment index (Figure 3F&G). There was no significant difference between two fiber diameters with the same spacing. On F/5-25 and F/10-25 matrices, the alignment on the top layer was hampered because too many cells packed on the top layer; however, the cells that penetrated and grew on the middle layer were still able to align due to the parallel topographic feature of fibers. On the other hand, on F/5-75 and F/10-75 matrices, cells grew and elongated along single fibers, which resulted in the best cell alignment. Although F/5-75 and F/10-75 matrices had highest CM alignment, the wider spacing compromised 3D tissue formation, thus 50 μm spacing matrices (F/5-50 and F/10-50) were used in the following experiments to determine the CM contractility.

3.4 Effect of fiber stiffness on CM contractility

CM contractility is the mechanical behavior resulting from the electrical activity, and the relationship between electrophysiology and contractility has been determined by simultaneously electrical measurement using the MED64 system and motion-tracking analysis using bright-field microscopy for video recording. The electrical waveform and the motion vectors were correlated to show that longer field potential duration resulted in the longer duration of entire contraction-relaxation. The LQT3 iPS-CMs with 400 ms FPD had the BD about 460 ms.

We then used real-time video recording and motion-tracking software to capture and analyze the beating behavior of LQT3 iPS-CM on the F/5-50 matrix (Figure 4A, Movie S4). The heatmap was plotted to visualize the spatial motion profile of CM beating on the filamentous matrix during the entire recorded video (Figure 4B). The area with highest mean motion velocity was selected to plot the motion-tracking waveform (Figure 4C). Using the waveform, we easily determined the maximal contraction velocity (MCV), maximal relaxation velocity (MRV) and beating duration (BD). The features of CM contractility (MCV, MRV, and BD) of WT and LQT3 iPS-CMs were compared between two matrices with different fiber diameters, F/5-50 and F/10-50 (Figure 4D-F). Because of the different stiffness of the fibers with different diameters, the beating CMs were able to deform the fibers on F/5-50 matrices, but not on F/10-50 matrices. Therefore, the MCV, MRV and BD of both cell types growing on F/5-50 matrices were larger than the ones growing on F/10-50 matrices. LQT3 and WT iPS-CMs growing on F/10-50 showed no significant difference in contractility, but LQT3 iPS-CMs growing on F/5-50 exhibited higher MCV and longer BD than WT iPS-CMs. Growing only on F/5-50 matrices, the LQT3 iPS-CMs exhibited contractility abnormality compared to WT iPS-CMs. Therefore, we used F/5-50 matrices in the following experiments to create tissue models from LQT3 iPS-CMs.

3.5 Drug testing on cardiac model

Once we had optimized the 3D cardiac tissue model for LQT3 iPS-CMs according to 3D tissue formation, CM alignment, and abnormality contractility, we then validated this model by testing the response of LQT3 iPS-CMs to different chemical compounds that had well-known effect on cardiac tissue (Table S3). After growing LQT3 iPS-CMs on F/5-50 matrices for 7 days, they were treated with two different doses of each compound, and CM responses were evaluated using real-time video recording and motion-tracking software to determine the contractility malfunctions (Figure 5). Caffeine is known to increase heart rate and enhance the internal Ca^{2+} release from the sarcoplasmic reticulum. Since intracellular Ca^{2+} transient is directly related to CM contractility, applying caffeine to our 3D cardiac tissue model with LQT3 iPS-CMs caused the BF and MCV to increase. A L-type Ca^{2+} channel blocker, nifedipine, decreased the BF and MCV, and increased the BD by decreasing CM Ca^{2+} influx. Higher doses of caffeine (500 nM) and nifedipine (300 nM) both caused LQT3 iPS-CMs to cease beating, but no uncoordinated beating resulting from arrhythmias was found via the motion-tracking waveform (Figure S2B&C). E4031, a hERG K^+ channel blocker, and propranolol, a beta-adrenergic antagonist showed similar effects on LQT3 iPS-CMs, decreasing BF and MCV and increasing the BD in a dose-dependent manner. E4031 caused a small level of irregular beating patterns shown in the baseline of the motion-tracking waveform (Figure S2D), but propranolol induced significant uncoordinated beating, suggestive of cardiac arrhythmias (Figure S2E).

To compare the drug response of LQT3 iPS-CMs between our 3D cardiac tissue model and traditional 2D cell culture, we grew LQT3 iPS CMs on 2D surfaces, F/5-50 matrices and F/10-50 matrices. We used 30 μM propranolol to treat these cells growing on different substrates and quantified the change in BF, MCV and BD due to the drug interference relative to control groups without any treatment. The change in CM contractility on F/5-50 matrices was significantly larger than F/10-50 matrices and 2D surfaces (Figure 6A-C), thus LQT3 iPS-CMs were more sensitive to the drug if they grew as a 3D tissue structure with low fiber stiffness. The change in MCV on F/10-50 matrices was larger than 2D surfaces, but no significant difference of BF and BD between these two substrates. We also quantified the percentage of uncoordinated beating within one motion-tracking waveform with different doses of propranolol (10 μM, 30 μM and 60 μM). The percentage of uncoordinated beating increased with the increasing propranolol concentration (Figure 6D) for all the substrates, but the difference was not significant among these substrates until the concentration was increased to 30 μM, at which time LQT3 iPS-CMs experienced more arrhythmias growing on F/5-50 matrices than F/10-50 matrices and 2D surfaces. At a concentration of 60 μM, about 70% beating of LQT3 iPS-CMs on F/5-50 became irregular and uncoordinated. The percentage of uncoordinated beating on F/5-50 was still the largest, and the percentage on F/10-50 also became significantly larger compared to the 2D surfaces. These results indicated that LQT3 iPS-CMs are more susceptible to cardiotoxicity caused by pharmacological interference when grown as 3D cardiac tissue with lower stiffness.

4. Discussion

As proof of principle to assess the susceptibility of cells exhibiting genetic cardiac disorders to drug-induced cardiotoxicity, we differentiated and characterized iPS-CMs with LQT3 syndrome, which were then used to test a panel of drugs known to affect cardiac electrophysiology. We have consistently been able to generate LQT3 iPS-CMs with 90% purity using a small molecule WNT-mediated differentiation protocol [18], and these diseased CMs were characterized via multiple cardiac specific markers and various experimental methods. They exhibited prolongation of QT interval compared to WT iPS-

CMs as observed by electrical field potential, which verifies that the LQT3 iPS-CMs can faithfully recapitulate the electrophysiological abnormality *in vitro*.

In the natural tissue environment, cells are surrounded by a 3D organization of supporting matrix and neighboring cells with gradients of chemical, electrical and mechanical signals. Creating a multicellular architecture with a highly controlled cellular microenvironment makes it possible to manufacture standardized *in vitro* models, which allow controlled modulation of various parameters (e.g. cellular composition, environmental factors) and are amenable to high-content drug screening and toxicity testing. *In vivo* CMs polarize their intracellular contractile apparatus and align with neighboring cells to facilitate the rapid spread of electrical activation and increase the contraction force [22,23]. Due to the difficulty of replicating such 3D aligned tissue microenvironment *in vitro*, cardiovascular pharmacology studies are particular challenging and may result in false readouts. The limitations of existing 2D cell culture practices have therefore provided an impetus for the development of alternative cell-based *in vitro* models that better mimic the complex cellular architectures and functions of living organs [24,25].

In this study, we used the TPIP technique to create a cohort of 3D filamentous matrices to regulate the structural organization of CMs and their functions. We successfully created TPIP matrices with different fiber diameters and spacing, and found that fiber spacing predominantly determined the formation of 3D tissue and CM alignment. The smaller 25 μm spacing hampered the immediate infiltration of CMs into the matrices necessary to create a true 3D cellular structure, and accumulation of CMs on the top layer created non-aligned 2D monolayer. The larger 75 μm spacing hampered the cell connections among multiple fibers, thus resulting in single-cell alignment along individual fiber instead of a condensed tissue structure. Therefore, we concluded that the matrices with intermediate fiber spacing, 50 μm, were best to generate 3D condensed cardiac tissue with proper CM alignment. It has been suggested that CM alignment involved with the CM contractile function and dysfunction in the cardiac tissue [26]. The parallel registration of sarcomeric Z-line and calcium metabolism were strongly correlated with the range of CM shapes [27], and cytoskeleton and sarcomeres play an important role in modulating ion channel kinetics and calcium transient [28]. The spatial alignment of CMs in our filamentous matrices enhanced the parallel coupling of myofibrils to maintain the polarity of the contractile apparatus of CMs and might eventually altered intracellular network responsible for the spatiotemporal coordination of cellular contractility.

These synthetic fibers serving as the backbone of the 3D cardiac tissue can be considered to mimic the perimysial collagen fibers of myocardium, since their physical dimensions and material properties correlate with CM alignment and contribute to myocardium nonlinear passive stiffness [29,30]. Therefore, the fiber stiffness can mimic the tissue stiffness of the 3D cardiac tissue and serve as the passive mechanical stimulus to the cells, which has been considered as one of the dominant factors in how cellular microenvironment regulates cell function. It has been reported that CMs were able to sense the local tissue stiffness through various cellular mechanotransduction pathways and consequently alter their electrophysiology and contractility [31,32]. By seeding and growing LQT3 iPS-CMs and WT iPS-CMs on F/5-50 and F/10-50 matrices, we found that beating iPS-CMs can easily bend the 5 μm fiber, but not the 10 μm fibers, and the iPS-CMs exhibited significantly more contractile motion on the F/5-50 matrices relative to what they exhibited on F/10-50 matrices. Interestingly, we observed that LQT3 iPS-CMs exhibited longer beat duration comparing to WT iPS-CMs only when growing on the matrices with lower stiffness, which suggested that variation of scaffold stiffness was required to facilitate monitoring of the genetic deficiency in LQT3 iPS-CMs. It is also possible that scaffold stiffness itself plays a role in this etiology. Our work suggested 3D *in vivo*-mimicking tissue structure with

physiological relevant stiffness represented more the dominantly diseased phenotype and might be essential for generating the *in vitro* model for understanding the mechanism of cardiac disease.

Although characterized by the same syndrome, patients with LQT1 (KCNQ1) and LQT2 (hERG) experience cardiac arrest due to exercise and emotion stress, but patients with LQT3 experience it with a slower heart rate during sleep and rest. Clinical evidence clearly indicates that only certain environmental conditions can amplify the electrophysiological disorder into the sudden heart dysfunction. Therefore, drug testing for LQT3 iPS-CMs in different cellular microenvironments may result in different pharmaceutical responses. Our findings indicated that LQT3 iPS-CMs became more susceptible to drug-induced cardiac toxicity growing on F/5-50 matrices compared to F/10-50 matrices and the pharmaceutical industry standard 2D surface as assessed by measurement of the beating duration and induction of uncoordinated beating, suggestive of cardiac arrhythmias. LQT3 iPS-CMs on F/5-50 matrices experienced a 40% higher risk of uncoordinated beating compared to 2D surfaces when treated with 60 μM propranolol. The high frequency of contractility malfunction observed in LQT3 iPS-CM on F/5-50 suggests that there might be false-negative readouts during toxicity testing if only traditional 2D cell culture systems are used for drug screening. Further drug testing on LQT3 iPS-CMs with other compounds showed that increased beating frequency by caffeine did not result in uncoordinated beating, which was consistent with clinical records of LQT3 patients who had cardiac arrest with slow heart rate. The L-type Ca^{2+} channel blocker, nifedipine, has been reported to shorten the CM action potential duration [33]. Conversely, its effect on LQT3 iPS-CMs on F/5-50 matrices was found to elongate the beating duration. This is likely the consequence of slow Ca^{2+} influx, which results in a longer release time of the internal Ca^{2+} stored in the SR necessary to complete the contraction. This phenomenon suggests CM contractility might not fully represent the CM electrophysiology, especially with drug interference. The hERG K^+ channel blocker E4031 has been known as the drug inducing severe arrhythmias, which was used in our study to test the cardiotoxicity tolerance and contractility malfunction of LQT3 iPS-CMs growing on F/5-50 filamentous matrices. We found that E4031 decreased the LQT3 iPS-CMs contractility, elongated the beating duration, and induced irregular contractions. The irregular movement between contraction and relaxation within one beat are most likely the result of early afterdepolarizations (EADs), and the ones between two beats are most likely the result of delayed afterdepolarizations (DADs). Propranolol is used to control the LQT1 and LQT2 syndrome by decreasing the heart beat rate, which has been proved with lethal effect for LQT3 patients. In our study, we found this drug induced uncoordinated beating, which was consistent with clinical cases.

The limitations of this 3D cardiac tissue model need to be stated. The CMs generated from iPS cells were immature embryonic or neonatal-like CMs, which morphologically cannot compare with large and stiff ventricular CMs in the adult human heart [34]. The cardiac tissue constructed by iPS-CMs had significantly lower field potentials and contraction forces than adult ventricular tissue and at this point cannot be considered an exact *in vitro* model of mature myocardium. Numerous studies have been published suggesting that CM alignment is beneficial to maturation [11,35], thus direct differentiation on 3D filamentous matrices, instead of replating CMs from the 2D differentiation system might help CM differentiation and maturation. Electrical stimulation would be an alternative method to help CM maturation [36], a long-term stimulation system is under development, which can adjust the magnitude and frequency of the electrical field. The filamentous matrices were fabricated between two glass plates, with the two ends of each fiber fixed on the glass. This design resulted in larger contractions of iPS-CMs perpendicular to the cell alignment direction, since the glass plates were too stiff to bend. We're developing a new filamentous matrix, in which the glass plates are replaced by pairs of flexible posts. A PDMS membrane has been

fabricated with an array of post pairs, and the fibers will be polymerized between each pair of PDMS posts. Therefore, CMs will be able to bend the posts and result higher contraction along the fiber direction, which is more precisely mimicking the physiological fashion.

5. Conclusion

We established an *in vitro* model of 3D human cardiac tissue by populating synthetic matrices with healthy WT and patient-specific LQT3 iPS-CMs. We determined the optimized fiber spacing as 50 μm for the 3D human cardiac tissue model by observing the formation of 3D tissue structure and CM alignment. We found that LQT3 iPS-CMs exhibited more contractility abnormality than WT iPS-CMs, and were more susceptible to drug-induced cardiotoxicity when grown on the filamentous matrices with low fiber stiffness compared to the matrices with high fiber stiffness and 2D surfaces. This highly defined human 3D cardiac model will help us better understand the LQT3 disease mechanism and formulate better therapeutic strategies for this syndrome. This model is also a pioneering testbed for assessing drug efficacy for patients with rare genetic disorders, moving drug discovery and development into the era of personalized medicine.

Supplementary Material

Refer to Web version on PubMed Central for supplementary material.

Acknowledgments

This work was supported by NIH-NHLBI R01HL096525, R01HL108677, U01HL100406, U01HL098179 and in part by NIH-NCATS UH2TR000487. Work at the Laser Thermal Laboratory was in part supported by the NSF (DMI-0556363). Z.M. would like to acknowledge Siebel Institute Postdoctoral Fellowship (41523-31595-44-OYZHMA-IQKEH). We acknowledge assistance from the Berkeley Stem Cell Shared Facility and Biological Imaging Facility.

References

1. Moretti A, Bellin M, Welling A, Jung CB, Lam JT, Bott-Flugel L, et al. Patient-specific induced pluripotent stem-cell models for long-QT syndrome. N Engl J Med. 2010; 363:1397–409. [PubMed: 20660394]
2. Itzhaki I, Maizels L, Huber I, Zwi-Dantsis L, Caspi O, Winterstern A, et al. Modelling the long QT syndrome with induced pluripotent stem cells. Nature. 2011; 471:225–9. [PubMed: 21240260]
3. Grskovic M, Javaherian A, Strulovici B, Daley GQ. Induced pluripotent stem cells – opportunities for disease modeling and drug discovery. Nat Rev Drug Discov. 2011; 10:915–29. [PubMed: 22076509]
4. Engler AJ, Sen S, Sweeney HL, Discher DE. Matrix elasticity directs stem cell lineage specification. Cell. 2005; 126:677–89. [PubMed: 16923388]
5. Hwang YS, Chung BG, Ortmann D, Hattori N, Moeller HC, Khademhosseini A. Microwell-mediated control of embryoid body size regulates embryonic stem cell fate via differential expression of WNT5a and WNT11. Proc Natl Acad Sci USA. 2009; 106:16978–83. [PubMed: 19805103]
6. Kilian KA, Bugarija B, Lahn BT, Mrksich M. Geometric cues for directing the differentiation of mesenchymal stem cells. Proc Natl Acad Sci USA. 2010; 107:4872–7. [PubMed: 20194780]
7. Eng G, Lee BW, Parsa H, Chin CD, Schneider J, Linkov G, et al. Assembly of complex cell microenvironments using geometrically docked hydrogel shapes. Proc Natl Acad Sci USA. 2013; 110:4551–6. [PubMed: 23487790]
8. Ma Z, Liu Q, Yang H, Runyan RB, Eisenberg CA, Xu M, et al. Laser patterning for the study of MSC cardiogenic differentiation at the single-cell level. Light Sci Appl. 2013; 2:e68.
9. Jacot JG, McCulloch AD, Omens JH. Substrate stiffness affects the functional maturation of neonatal rat ventricular myocytes. Biophys J. 2008; 95:3479–87. [PubMed: 18586852]

10. Galie PA, Khalid N, Carnahan KE, Westfall MV, Stegemann JP. Substrate stiffness affects sarcomere and costamere structure and electrophysiological function of isolated adult cardiomyocytes. Cardiovasc Pathol. 2013; 22:219–27. [PubMed: 23266222]
11. Schaaf S, Shibamiya A, Mewe M, Eder A, Stohr A, Hirt MN, et al. Human engineered heart tissue as a versatile tool in basic research and preclinical toxicology. PLoS One. 2011; 6:e26397. [PubMed: 22028871]
12. Boudou T, Legant WR, Mu A, Borochin MA, Thavandiran N, Radisic M, et al. A microfabricated platform to measure and manipulate the mechanics of engineered cardiac microtissues. Tissue Eng Part A. 2012; 18:910–9. [PubMed: 22092279]
13. Liau B, Christoforou N, Leong KW, Bursac, N. Pluripotent stem cell-derived cardiac tissue patch with advanced structure and function. Biomaterials. 2011; 32:9180–7. [PubMed: 21906802]
14. Orlova Y, Magome N, Liu L, Chen Y, Agladze K. Electrospun nanofibers as a tool for architecture control in engineered cardiac tissue. Biomaterials. 2011; 32:5615–24. [PubMed: 21600646]
15. Dong X, Zhao Z, Duan X. Improving spatial resolution and reducing aspect ratio in multiphoton polymerization nanofabrication. Appl Phys Lett. 2008; 92:091113.
16. Jeon H, Hidai H, Hwang DJ, Healy KE, Grigoropoulos CP. The effect of micronscale anisotropic cross patterns on fibroblast migration. Biomaterials. 2010; 31:4286–95. [PubMed: 20189640]
17. Koroleva A, Gill AA, Ortega I, Haycock JW, Schlie S, Gittard SD, et al. Two-photon polymerization-generated and micromolding-replicated 3D scaffolds for peripheral neural tissue engineering applications. Biofabrication. 2012; 4:025005. [PubMed: 22522957]
18. Lian X, Hsiao C, Wilson G, Zhu K, Hazeltine LB, Azarin SM, et al. Robust cardiomyocyte differentiation from human pluripotent stem cells via temporal modulation of canonical Wnt signaling. Proc Natl Acad Sci USA. 2012; 109:1848–57.
19. Zhu WZ, Van Biber B, LaFlamme MA. Methods for the derivation and use of cardiomyocytes from human pluripotent stem cells. Methods Mol Biol. 2011; 767:419–31. [PubMed: 21822893]
20. Xu J, Po L, Cheung C. Adaptive motion tracking block matching algorithms for video coding. IEEE Trans Circuits Syst Video Technol. 1999; 9:1025–29.
21. Hutter JL, Bechhoefer J. Calibration of atomic-force microscope tips. Rev. Sci. Instrum. 1993; 64:1868–73.
22. Ma Z, Liu Q, Liu H, Yang H, Yun JX, Eisenberg C, et al. Laser-patterned stem-cell bridges in a cardiac muscle model for on-chip electrical conductivity analyses. Lab Chip. 2012; 12:566–73. [PubMed: 22170399]
23. Grosberg A, Alford PW, McCain ML, Parker KK. Ensembles of engineered cardiac tissues for physiological and pharmacological study: heart on a chip. Lab Chip. 2011; 11:4165–73. [PubMed: 22072288]
24. Sung JH, Esch MB, Prot JM, Long CJ, Smith A, Hickman JJ, et al. Microfabricated mammalian organ systems and their integration into models of whole animals and humans. Lab Chip. 2013; 13:1201–12. [PubMed: 23388858]
25. Sung JH, Shuler ML. Microtechnology for mimicking *in vivo* tissue environment. Ann Biomed Eng. 2012; 40:1289–300. [PubMed: 22215276]
26. Gerdes AM, Capasso JM. Structural remodeling and mechanical dysfunction of cardiac myocytes in heart failure. J Mol Cell Cardiol. 1995; 27:849–56. [PubMed: 7602601]
27. Kuo PL, Lee H, Bray MA, Geisse NA, Huang YT, Adams WJ, et al. Myocyte shape regulates lateral registry of sarcomeres and contractility. Am J Pathol. 2012; 181:2030–7. [PubMed: 23159216]
28. Prosser BL, Ward CW, Lederer WJ. X-ROS signaling: rapid mechano-chemo transduction in heart. Science. 2011; 333:1440–5. [PubMed: 21903813]
29. Pope AJ, Sands GB, Smaill BH, LeGrice IJ. Three-dimensional transmural organization of perimysial collagen in the heart. Am J Physiol Heart Circ Physiol. 2008; 295:1243–52.
30. Mackenna DA, Vaplon SM, McCulloch AD. Microstructural model of perimysial collagen fibers for resting myocardial mechanics during ventricular filling. Am J Physiol. 1997; 273:1576–86.
31. Forte G, Pagliari S, Ebara M, Uto K, Tam JK, Romanazzo S, et al. Substrate stiffness modulates gene expression and phenotype in neonatal cardiomyocytes *in vitro*. Tissue Eng Part A. 2012; 18:1837–48. [PubMed: 22519549]

32. Bhana B, Iver RK, Chen WL, Zhao R, Sider KL, Likhitpanichkul M, et al. Influence of substrate stiffness on the phenotype of heart cells. Biotechnol Bioeng. 2010; 105:1148–60. [PubMed: 20014437]

33. Zhang GQ, Wei H, Lu J, Wong P, Shim W. Identification and characterization of calcium sparks in cardiomyocytes derived from human induced pluripotent stem cells. PLoS One. 2013; 8:e55266. [PubMed: 23408964]

34. Lundy SD, Zhu WZ, Regnier M, Laflamme MA. Structural and functional maturation of cardiomyocytes derived from human pluripotent stem cells. Stem Cell Dev. 2013; 22:1991–2002.

35. Zhang D, Shadrin IY, Lam J, Xian HQ, Snodgrass HR, Bursac N. Tissue-engineered cardiac patch for advanced functional maturation of human ESC-derived cardiomyocytes. Biomaterials. 2013; 34:5813–20. [PubMed: 23642535]

36. Nunes SS, Miklas JW, Liu J, Aschar-Sobbi R, Xiao Y, Zhang B, et al. Biowire: a platform for maturation of human pluripotent stem cell-derived cardiomyocytes. Nat Methods. 2013; 10:781–7. [PubMed: 23793239]

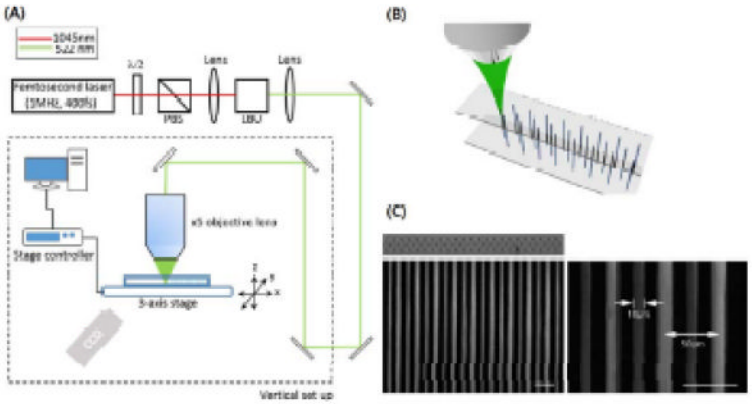

Figure 1.

(A) Schematic of TPIP system to fabricate the filamentous matrices; (B) Schematic of TPIP fabrication process to polymerize fibers with highly defined diameter and spacing; (C) SEM images of a fabricated F/10-50 filamentous matrix. (Scale bar: 50 μm)

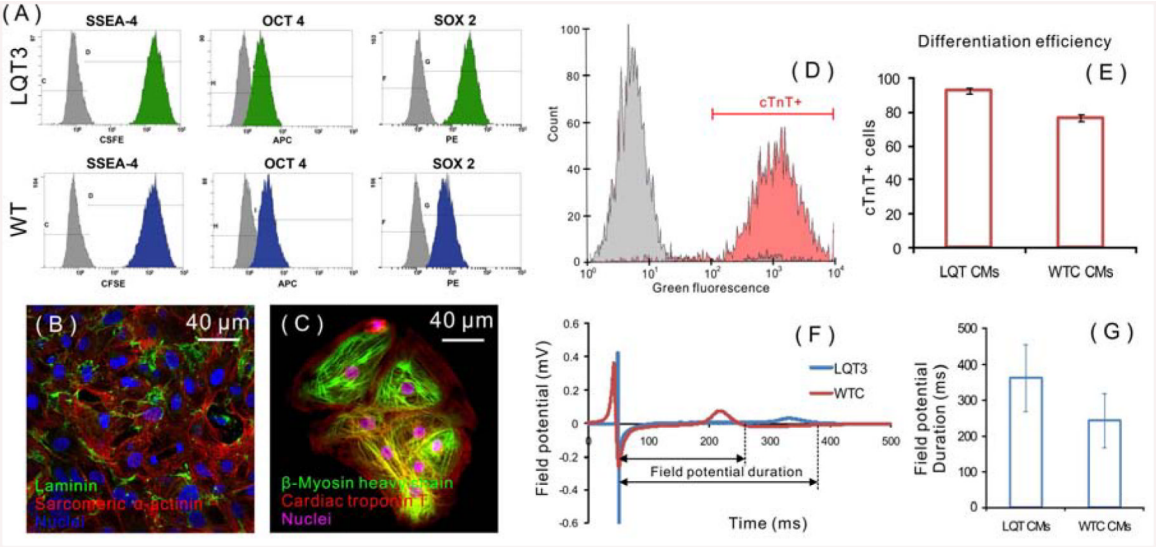

Figure 2.

(A) Characterization of LQT3 and WT iPS cells with pluripotent markers SSEA4, Oct4 and Sox2 with flow cytometry method. The differentiated LQT3 iPS-CMs expressed cardiac specific markers: (B) sarcomeric α-actinin and (C) cardiac troponin T (cTnT) and β-myosin heavy chain. The differentiation efficiency was characterized using flow cytometry method, and histogram (D) showed that the selected cTnT+ population (red) represented the CMs relative to isotype control (grey). (E) We obtained about 90% purity for LQT3 iPS-CMs differentiation and 75% purity for WT iPS-CMs differentiation. (F) The waveforms of field potentials measured using MEA system were plotted and showed elongated FPD of LQT3 iPS-CMs comparing to WT iPS-CMs. (G) We found the average FPD for LQT3 iPS-CMs was ~370 ms, whereas WT iPS-CMs was ~250 ms.

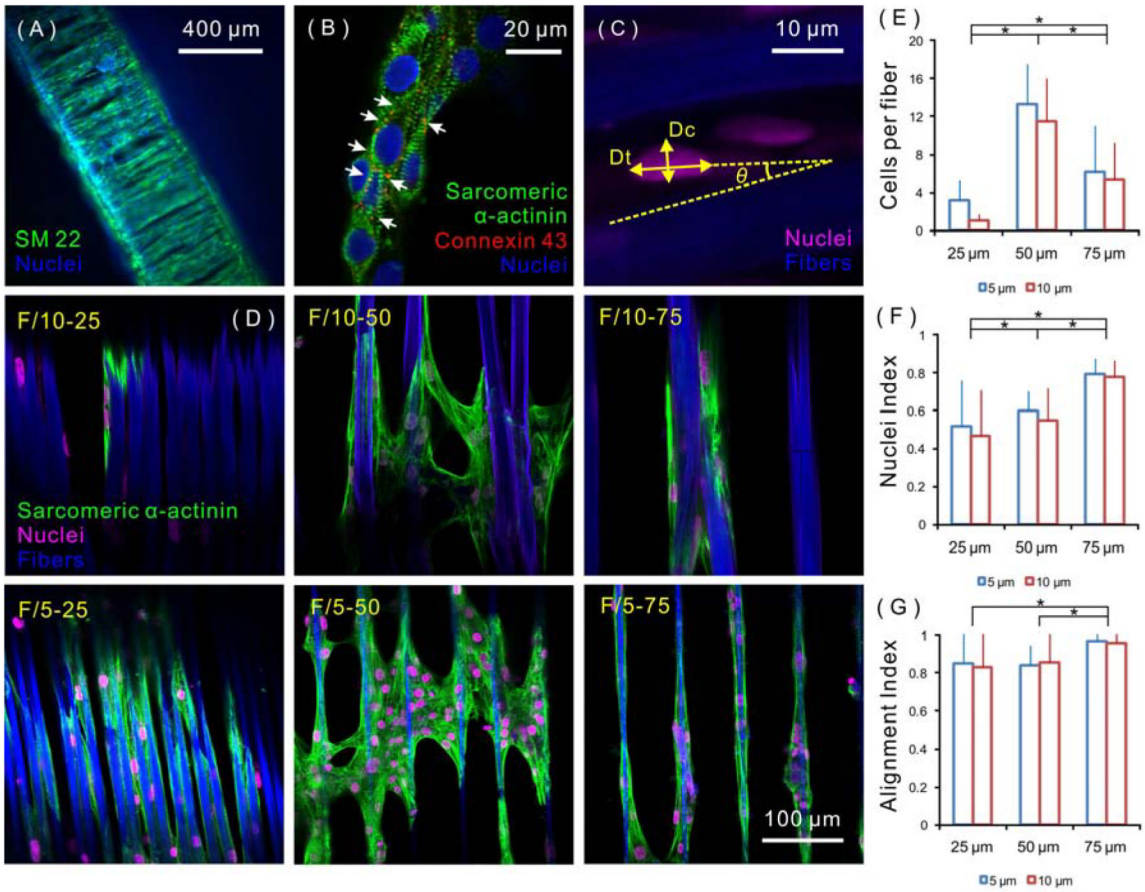

Figure 3.

(A) The entire 3D condensed cardiac tissue was visualized by staining SM22, which was positive for both CMs and myofibroblasts. (B) Confocal images of CMs aligned on one fiber showed the sarcomere structure stained by sarcomeric α-actinin and intercellular gap junctions stained by connexin 43, which ensured the electrical integration within the cardiac tissue (white arrow pointing to connexin43 staining). (C) Confocal images showed the cell nuclei within the filamentous matrix, and the parameters used for calculation of nuclei index and alignment index. (D) The confocal images for LQT3 iPS-CMs growing on the middle layer of filamentous matrices and aligning along the fiber direction with different fiber diameters and spacing. The formation of 3D cardiac tissue was quantified by the cell number on the middle layer relative to the fiber number, and we found (E) matrices with 50 μm fiber spacing resulted in highest value of cell per fiber. The CM alignment was quantified by (F) nuclei index and (G) alignment index, and we found matrices with 75 μm fiber spacing resulted in highest value of CM alignment. (*$p<0.05$, N=10)

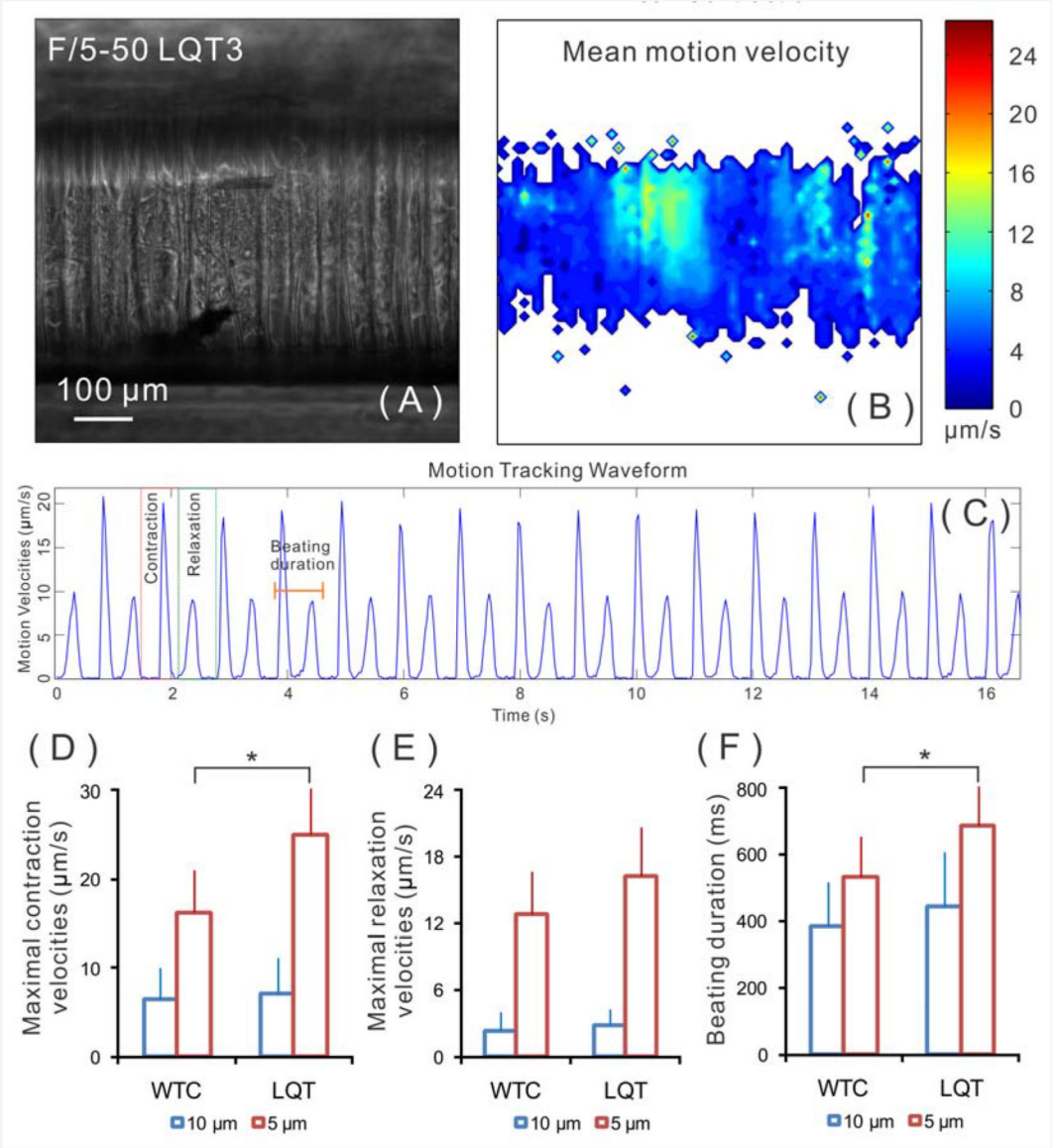

Figure 4.

(A) LQT3 iPS-CMs grew as 3D condensed cardiac tissue on a F/5-50 filamentous matrix and were able to spontaneously beat, which was captured and analyzed by motion-tracking software. (B) The heatmap was plotted to show the area with highest mean motion velocity during the entire recorded video. (C) In the motion tracking waveform, we can easily identify the contraction and relaxation during one CM beating and measure the beating duration. According to motion tracking waveform, iPS-CMs on F/5-50 matrices had higher (D) MCV, (E) MRV, and (F) BD than the ones on F/10-50 matrices, and LQT3 iPS-CMs exhibited significant higher (D) MCV and (F) BD than WT iPS-CMs only on F/5-50 matrices. (*$p<0.05$, N=10)

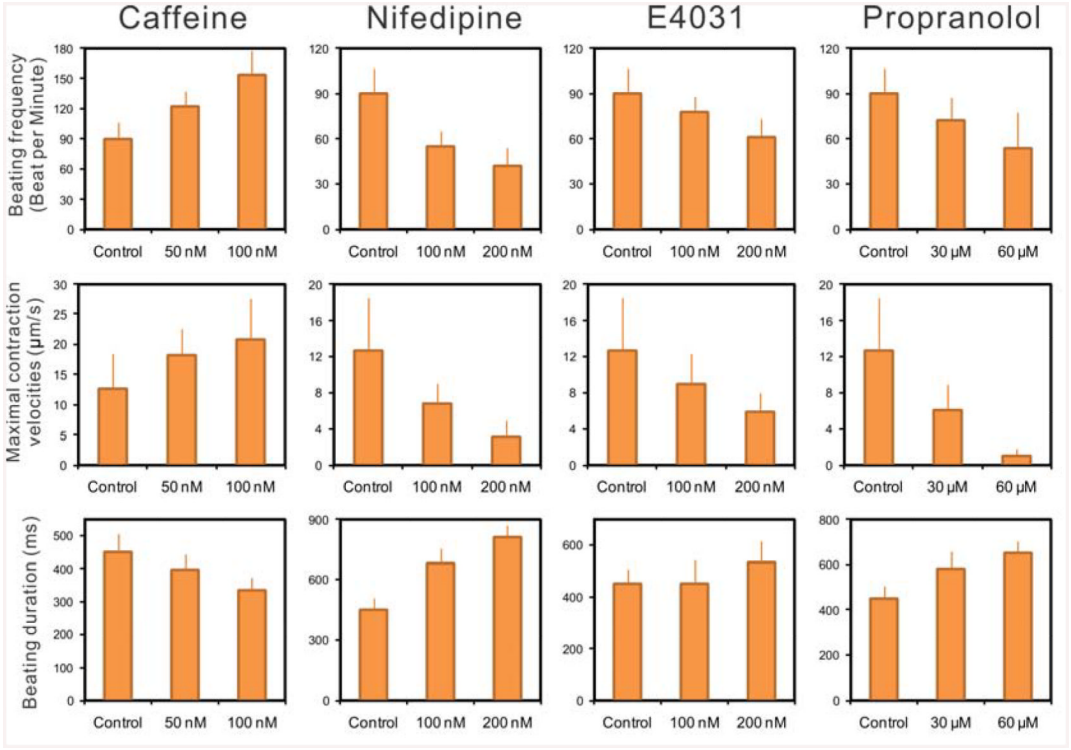

Figure 5.

The LQT3 iPS-CMs on F/5-50 matrices were tested the contractility changes (BF, MCV, and BD) to four different compounds, caffeine, nifedipine (L-type Ca^{2+} channel blocker), E4031 (hERG K^{+} channel blocker) and propranolol (β-adrenergic antagonist). Caffeine increased the CMs contractility, whereas the other three compounds decreased the contractility at a dose-dependent manner.

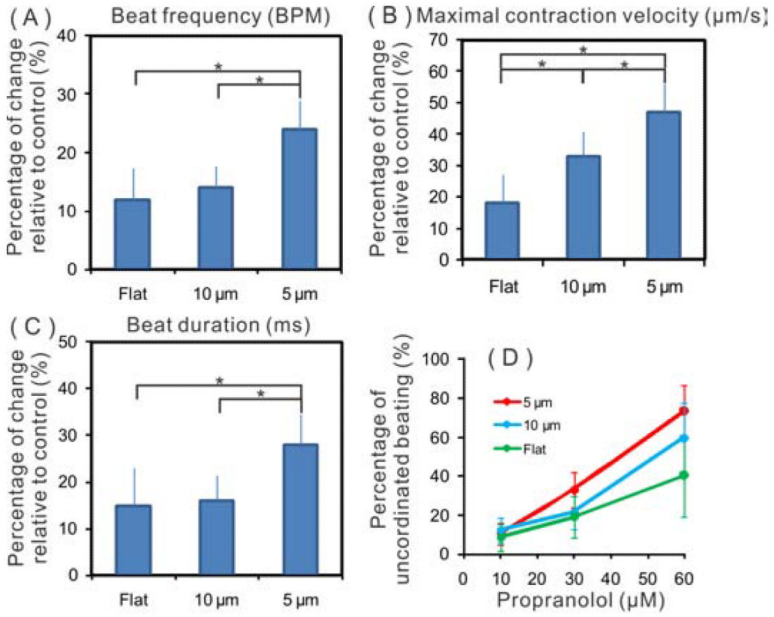

Figure 6.

The LQT3 iPS-CMs response to 30 μM propranolol was tested on three different substrates: 2D surfaces; F/10-50 matrices; and F/5-50 matrices. The change of (A) BF, (B) MCV and (C) BD resulted from drug treatment was calculated relative to control groups without treatment, and LQT3 iPS-CMs experienced higher changes on F/5-50 matrices than 2D surfaces and F/10-50 matrices. (D) The uncoordinated beating was counted within individual trace of motion tracking waveform for three different substrates with different dose of propranolol (10 μM, 30 μM and 60 μM).

Table 1

Calculated elastic modulus of the fibers within the filamentous matrices

Diameter (μm)	Elastic modulus (MPa)
5	158.06 ± 9.14
10	598.31 ± 86.17